Highly sensitive naked eye detection of Iron (III) and H_2O_2 using poly-(tannic acid) (PTA) coated Au nanocomposite

Yan Fang[a,b]**, Jiajun Tan[b]**, Hyunjun Choi[c], Sierin Lim[b,d], Dong-Hwan Kim[c]*

[a]State Key Laboratory of Materials-Oriented Chemical Engineering, College of Biotechnology and Pharmaceutical Engineering, Nanjing Tech University, Nanjing, 211816, People's Republic of China

[b]School of Chemical and Biomedical Engineering, Nanyang Technological University, 70 Nanyang Drive, Block N1.3, Singapore 637457

[c]School of Chemical Engineering, Sungkyunkwan University, 16419, Republic of Korea

[d]NTU-Northwestern Institute for Nanomedicine, Nanyang Technological University, 50 Nanyang Drive, Singapore 6374553

*Email: dhkim1@skku.edu

** Equal contribution to this work.

ABSTRACT

In the present study, we present a room temperature-, one-pot method for the synthesis of functional poly (tannic acid) (PTA)-based core@shell nanocomposites (core@PTA). The addition of tannic acid (TA) to gold (Au) salt solutions at mildly alkaline pH induced reduction of the metal salts to Au nanoparticles (NPs) while TA was oxidized and self-polymerized before encapsulating the AuNPs to form Au@PTA. Through the use of coordination chemistry, the synthesized Au@PTA was utilized as a naked eye sensor for iron (III) ions and H_2O_2. In the presence of Fe^{3+}, Au@PTA aggregated and resulted in visible color change, showing high selectivity towards Fe^{3+} with visual detection limit of 20 μM. Extension of the approach is used to detect H_2O_2 with visual detection limit of 0.4 μM. Observation of the UV-vis spectra after the addition of analytes for the two detection systems revealed an additional peak in the H_2O_2 detection system at ~ 650 nm. This is due to the presence of "wire-like" oligomer structures in the H_2O_2 detection system as opposed to nanocomposite aggregation observed in the former system.

KEYWORDS: tannic acid (TA); visual detection; naked eye; Fe^{3+}; H_2O_2; core@shell nanocomposites;

Introduction

Polymer coated metal nanoparticles (metal@polymer) are preferred over the nanoparticles capped with stabilizing agents from the point of view of stability and dispersion.[1] However, current methods of synthesizing metal@polymer nanocomposites not only require energy input but also are done in multiple steps. Usually, for the synthesis of metal@polymer nanocomposites, two reaction steps are generally required: the reduction of the metal ions to form the core, and subsequent shell formation through thiol-metal binding or covalent polymerization.[2-4] Here, we hypothesized that polyphenols capable of undergoing oxidative self-polymerization could self-assemble polymeric shells of metal@polymer nanocomposites in a single step without the need of cross-linkers or UV radiation.

One such poly-phenolic material would be tannic acid (TA). TA has been shown to undergo oxidative self-polymerization to poly-tannic acid (PTA) before coating onto graphene oxide surface.[5] Furthermore, tannic acid has also been used as a sole reducing and capping agent in heating-free green synthesis of metal nanoparticles.[6, 7] These two properties make tannic acid an advantageous candidate for the synthesis of metal@polymer nanocomposite.[8] Nevertheless, current methods of synthesizing metal@polyphenol nanocomposite with tannic acid shell as described by Zeng et al. still relied on iron (III) ions to induce coordination between TA to form the shell.[9]

Here we show that metal@polymer nanocomposite with PTA shell can be synthesized without any cross-linkers. As proof of concept, gold (Au) was used in our experiment to form the metal core of our metal@polymer nanocomposite. The

gold@poly-tannic acid (Au@PTA) was further applied as a sensor to detect the presence of iron (III) ions as well as hydrogen peroxide (H_2O_2).

Various elements, such as carbon, oxygen and hydrogen are necessary for the survival of living organisms. Particularly, iron is considered an indispensable element for life. It exists in both ferrous (Fe^{2+}) and ferric (Fe^{3+}) states to perform various biological functions.[10, 11] Many cellular processes, such as oxygen transportation and DNA synthesis, involve electron transfer between the two iron oxidation states.[12, 13] Iron levels are also crucial in biochemical, pharmacological, and toxicological functions in biological systems. Iron deficiency or iron overload can lead to various disorders and diseases.[14, 15] As such, much effort has been made to develop techniques for iron detection. These include absorbance measurements,[16] electrochemistry techniques,[17] magnetic resonance imaging,[18] high-performance liquid chromatography,[19] and fluorescence.[20] However, these methods are inconvenient as they require the use of measuring instruments. In this work, we have developed a simple and highly visual method for detecting Fe^{3+}. This technique relies on Au@PTA aggregation in aqueous solutions using coordination chemistry between PTA and Fe^{3+}. Fe^{3+} coordinates with the three galloyl groups in TA to form a stable octahedral complex and cross-linked structure, resulting in Au@PTA aggregation. The aggregation in turn gave rise to our read-out which was an observable naked eye color change. H_2O_2 plays an important role as an intermediate chemical in various industrial fields, such as food[21], pharmaceutical[22], clinical[23], and for environmental analysis[24]. As such a convenient and highly sensitive detection method is required to examine the presence of H_2O_2. By utilizing H_2O_2 to

oxidize Fe^{2+} to Fe^{3+}, we could induce the aggregation of Au@PTA, thus signaling the presence of H_2O_2.

Results and discussion

Synthesis of Au@PTA nanocomposite

Au@PTA nanocomposite was synthesized by one-pot synthesis mixing of Au^{3+} and TA under mildly alkaline condition. The TEM image (Figure 1a) showed that Au@PTA nanocomposites comprised two components with distinct electronic densities as compared with bare gold nanoparticles (AuNPs) (Figure 1a, inset).[9] The average diameter of the core of Au@PTA was ~ 20 nm, while the shell thickness was ~ 5 nm. The solution of Au@PTA nanocomposites exhibited a red color similar to that of typical Au colloids.[25-27] The UV-Vis spectra of an Au@PTA solution showed an extinction peak at around 550 nm (Figure 1b). The slight red-shift in the extinction peak of Au@PTA in comparison with that of 20 nm AuNPs (extinction peak of ~ 520 nm) was due to the increase of refractive index around AuNPs arising from the PTA coating on AuNPs.[9, 28] The corresponding element linear mapping of a single nanocomposite (Figure 1c, d) showed the distribution of the various elements in the nanocomposite, comprising Au (green), C (red), and O (black), indicating that the nanocomposites were composed of Au at its core and PTA as its shell.[29] Fourier transform infrared (FTIR) spectra confirmed that TA was oxidized by $HAuCl_4$ (Figure S1), which was in good agreement with previous reports.[30] Integration of the PTA shell onto the surface of the Au cores decreased the zeta potential from -11.5 ± 0.5 mV to -17.2 ± 0.5 mV due to the presence of acidic galloyl groups in TA (Table S1).

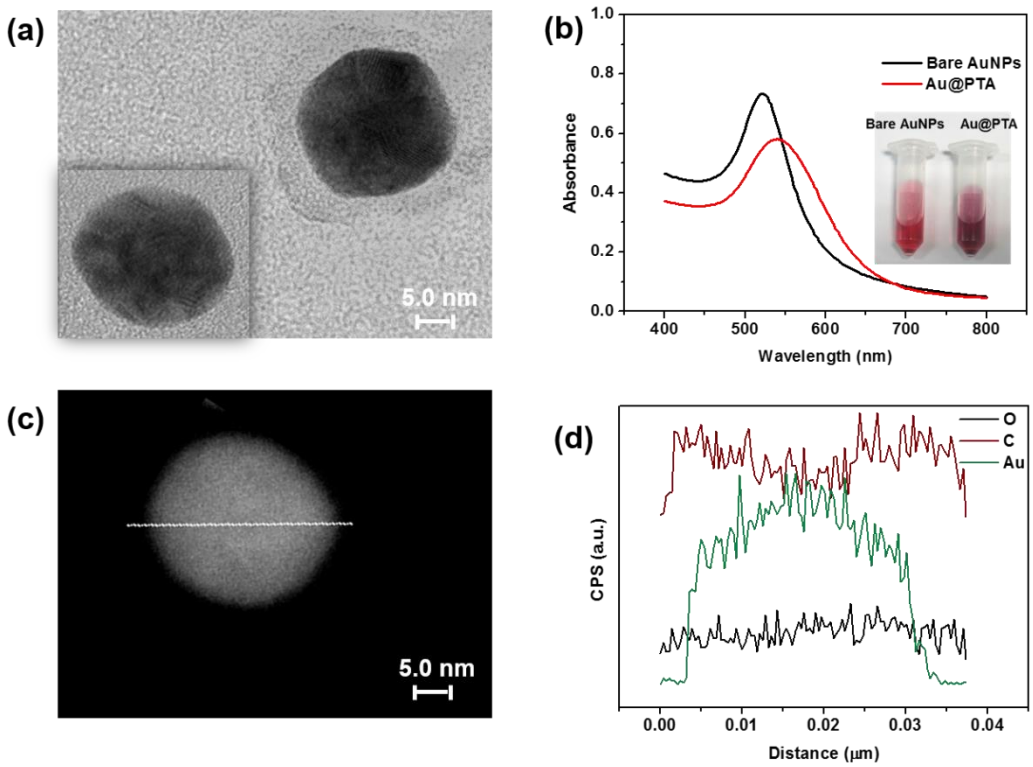

Figure 1. (a) TEM images of the bare AuNPs (the inset image) and Au@PTA; (b) UV-Vis spectra of the dispersed suspensions of bare AuNPs and Au@PTA. The inset is its optical image (c) STEM image of a single Au@PTA nanoparticle; (d) relevant element linear mapping: Au, C, and O.

To determine the optimal pH for Au@PTA synthesis, we carried out experiments to synthesize the Au@PTA in various pH conditions. The estimated pKa value of TA is 8.5.[31] TA monomer was stable in solutions at pH ≤ 7.0 because oxidation of TA is inhibited in acidic condition. However, TA solutions underwent oxidation at pH > 7.0 with atmospheric oxygen. When such oxidation occurs, self-polymerization of TA will take place spontaneously, causing the TA solution to turn faint yellow (Figure S2). Based on this observation, it could be inferred that, for each Au@PTA nanocomposite, TA were cross-linked through oxidation by $HAuCl_4$ and oxygen dissolved in the solution before self-assembling into the shell surrounding the AuNP cores. In this manner, the Au@PTA nanocomposites can be synthesized in a fast, one-pot synthesis pathway. Nevertheless, if

the pH of the solution was high (i.e., pH > 8.5), the speed of TA oxidation and self-polymerization would be too fast and the polymerized TA would be further oxidized and disassembled into smaller soluble molecules.[32] As a result, the shell would be unable to assemble on the AuNP core and the core@shell structure would not be formed. We determined that the optimal pH for Au@PTA nanocomposite synthesis to be pH = 7.8 (Table S2).

Time-course experiment was conducted to determine the growth mechanism of Au@PTA nanocomposites by monitoring the morphology of the nanocomposites using TEM at synthesis time points of 5, 10 and 20 min. Similar to other nanoparticle synthesis techniques, the electronic density at the beginning of the synthesis process (5 min) was not uniform and the nanoparticles aggregated in a "like-attracts-like" manner (Figure 2a). The white halo around the nanoparticles may be attributed to the presence of partially polymerized PTA. We may attribute the "like-attracts-like" aggregation of nanoparticles to the fusion between metal nanoclusters, which would grow into larger mesocrystals, as observed in many biomineralization processes.[33-35] At 10 min, although we observed capping of PTA onto the mesocrystals, uniformed Au@PTA nanocomposites were still not fully assembled (Figure 2b). After 20 min, capping of PTA is completed and a shell of thickness of ~5 nm was observed around the Au core (Figure 2c).

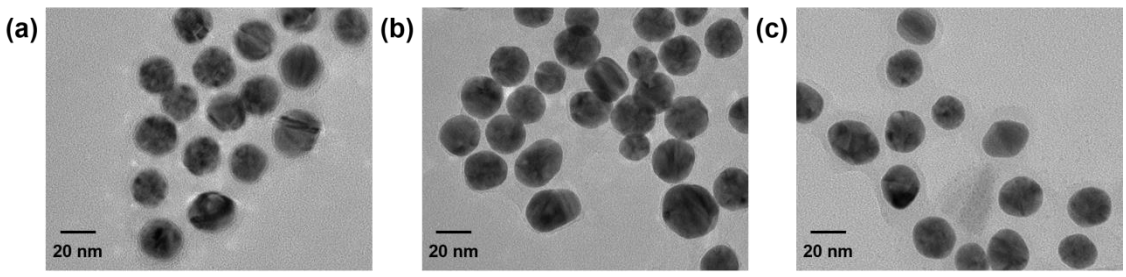

Figure 2. TEM images of Au@PTA nanocomposites collected at different times during the preparation process under pH = 7.8: (a) 5 min, (b) 10 min, and (c) 20 min.

Detection of Fe^{3+}

The synthesized Au@PTA was applied as a sensor to detect iron (III) ions. When Fe^{3+} was added to the Au@PTA solutions at room temperature, the color changed from red to blue (Figure 3a), and UV-Vis spectroscopy showed an absorption band shift from 550 nm to 600 nm which was caused by the aggregation of Au@PTA (Figure 3b, Figure S3). As the process of the resulting color change due to this aggregation can be monitored with naked eye alone, usage of instruments can be eliminated for the detection of Fe^{3+}.

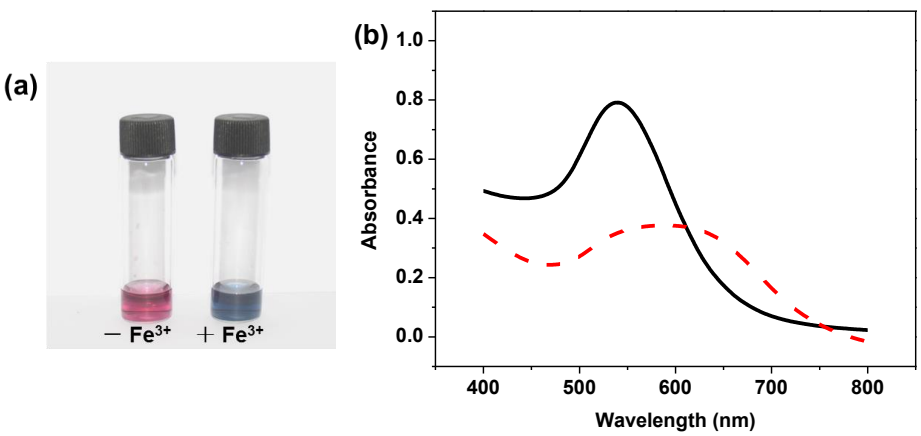

Figure 3. Assay for Fe^{3+} ions by naked eye (a) Photograph of the solution containing only Au@PTA nanocomposites (left) and the same solution after the addition of Fe^{3+} (20 μM) (right); (b) UV-Vis spectra obtained from solutions of Au@PTA nanocomposites and after 30 min incubation with Fe^{3+}. Solid black line: Au@PTA nanocomposites without Fe^{3+}, dashed red line: Au@PTA nanocomposites + Fe^{3+}.

To evaluate the minimum aqueous concentration of Fe^{3+} ions required for visible color change, we added Fe^{3+} into the Au@PTA solution at final Fe^{3+} concentrations ranging from 5 μM to 400 μM (Figure 4). After 5 min of reaction time, the results showed obvious color changes when [Fe^{3+}] ≥ 20 μM (Figure 3a), whereas distinct visible changes

of the solution color were not observed when [Fe^{3+}] < 5 μM (Figure S4). To our knowledge, our system offers the lowest detection limit for the visual detection of Fe^{3+} ions.[17-20]

Upon analysis of the UV-vis spectra of Au@PTA incubated at varying Fe^{3+} concentrations, we observed two sets of dynamic ranges (Figure 4a). Between concentrations of 5 μM and 40 μM, the increase in Fe^{3+} concentrations corresponded linearly to an increase in red-shift of the peak up to a maximum of 50 nm (Figure 4b). From Fe^{3+} concentrations of 40 μM to 200 μM, we observed that the intensity of absorbance at 600 nm (A_{600}) decreased linearly as the Fe^{3+} concentration increased (Figure 4c). This difference was due to the nature of aggregation that had taken place. Below concentrations of 40 μM, coordinate bonds between Fe^{3+} and Au@PTA resulted in the formation of small perforated aggregates. However, above 40 μM concentrations, not only did these small perforated aggregates form, they also clustered together to form larger aggregates. Hence, the difference in the dynamic ranges observed.

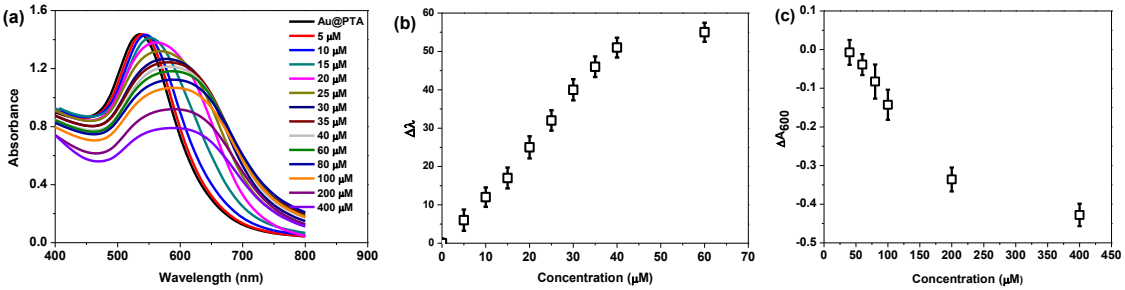

Figure 4. (a) UV-Vis spectra obtained from solutions of functionalized Au@PTA nanocomposites after adding different concentrations of Fe^{3+}. (b) A calibration curve corresponding to part a (5 - 60 μM). (c) A calibration curve corresponding to part a (40 - 200 μM). Values were normalized by subtracting from the A_{600} value at 35 μM Fe^{3+} concentration. The error bars represent the standard deviations of three replicates.

We also tested the selectivity of this assay for Fe^{3+} ions by replacing Fe^{3+} (20 μM) with other mono-, di-, or trivalent ions at final concentrations of 50 μM. Results show that only the sample containing Fe^{3+} induced a noticeable color change in Au@PTA (Figure 5 and Figure S5). None of the other metal ions interfered with the assay. Even when the concentrations of these ions were increased to 10 times the concentration of Fe^{3+} added (i.e., up to 200 μM) no distinct visible color changes or precipitates were observed in the Au@PTA solutions (data not shown). Furthermore, no color changes (except for Ag^{+} and Hg^{2+}) or aggregations were observed after incubating the samples for four weeks, indicating the long term stability of the Au@PTA based detection system. Conclusively, Au@PTA can be conveniently used to visually detect Fe^{3+}in a highly sensitive and selective manner.

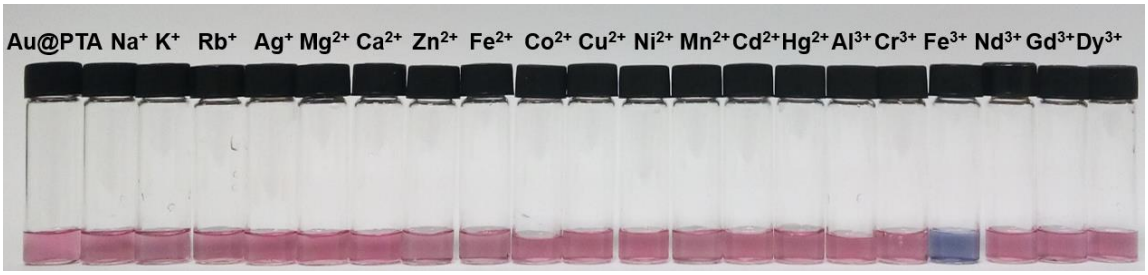

Figure 5. A photograph of the solutions containing the functionalized Au@PTA nanocomposites with different metal cations. Ion concentration of Na^{+}, K^{+}, Rb^{+}, Ag^{+}, Mg^{2+}, Ca^{2+}, Zn^{2+}, Fe^{2+}, Co^{2+}, Cu^{2+}, Ni^{2+}, Mn^{2+}, Cd^{2+}, Hg^{2+}, Al^{3+}, Cr^{3+}, Nd^{3+}, Gd^{3+}, and Dy^{3+} is 50 μM. [Fe^{3+}] = 20 μM.

Detection of H_2O_2

In addition to Fe^{3+}, we also expanded the method to detect (H_2O_2). H_2O_2 is an important intermediary chemical in various industries. Hence, its visual detection is advantageous for use in resource-scarce regions. As H_2O_2 is able to oxidize Fe^{2+} to Fe^{3+} (Equation (1)), it presents an attractive extension usage to our detection system. Fe^{3+}

produced from the oxidation of Fe^{2+} when H_2O_2 was added formed coordination bonds with the galloyl groups of the PTA shell causing the Au@PTA to aggregate immediately (Figure S6 - S7). When H_2O_2 or Fe^{2+} was added separately to the Au@PTA mixture, no color changes in the assay were observed even after 30 min. However, when H_2O_2 and Fe^{2+} ions were added together in the assay system, the color of Au@PTA solution turned blue (Figure 6a). The presence of Fe^{2+} was crucial for the assay to detect H_2O_2. UV-Vis spectroscopy analysis showed that the absorbance at 550 nm decreased and the peak broadened with marked increase at ~ 650 nm (red trace in Figure 6b).

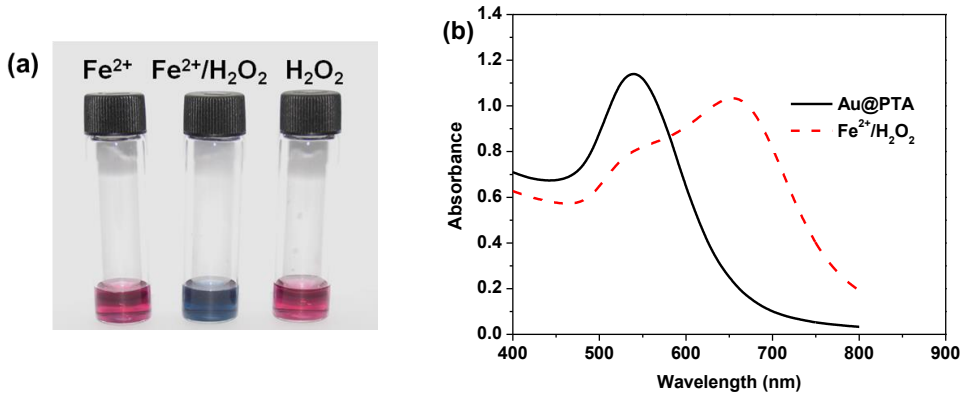

Figure 6. (a) Photograph of Au@PTA nanocomposites after adding Fe^{2+} (20 μM) with no oxidant, Fe^{2+} (20 μM) with H_2O_2 as the reductant, and H_2O_2, with no Fe^{2+}. (b) UV-Vis spectra obtained from solutions of functionalized Au@PTA nanocomposites and after 30 min in the presence of Fe^{2+} and H_2O_2. Solid line: Au@PTA nanocomposites, dotted line: Au@PTA nanocomposites + Fe^{2+}/H_2O_2.

We also investigated the sensitivity of our Au@PTA-based sensor for the detection of H_2O_2 by adding aliquots containing varying concentrations of the analyte H_2O_2 into Au@PTA nanocomposite solutions mixed with Fe^{2+}, and observed the result both visually and with the use of spectrometry. As observed in Figure 7a, the minimum concentration of H_2O_2 required for the Au@PTA solution to turn visibly blue was 0.4 μM. Between H_2O_2

concentrations of from 0.4 μM to 2.0 μM, an increase in the intensity of blue color was seen as the added H_2O_2 concentration increased. Our naked eye H_2O_2 minimum detection concentration of 0.4 μM was lower than the reported minimum visual detection limit for H_2O_2 concentration of 0.5 μM reported in the horseradish peroxidase-dependent nanoflower system developed by Lin et al.[29] To our knowledge, this makes our system the lowest detection level via naked eye visualization.[21-24]

By observing the UV-vis spectrum with varying concentrations of H_2O_2 added, we observed that our assay allowed for a large linear dynamic range between H_2O_2 concentrations of 10 nM and 1400 nM. We observed that the absorbance at ~ 650 nm increased linearly as the concentration of H_2O_2 increased (Figure 7c). Our assay's linearly dynamic range was much wider as compared to other previously reported sensors (2.5 - 11.2 mM,[21] 0.979 - 17.6 mM,[23] and 0.02 - 0.5 mM[29]) when similar experimental conditions were used for H_2O_2 detection. As the H_2O_2 concentration reached a saturation limit 1.4 μM in our assay, the normalized absorbance at 650 nm increases at a slower rate as compared to between concentrations of 10 nM and 1400 nM (Figure 7c).

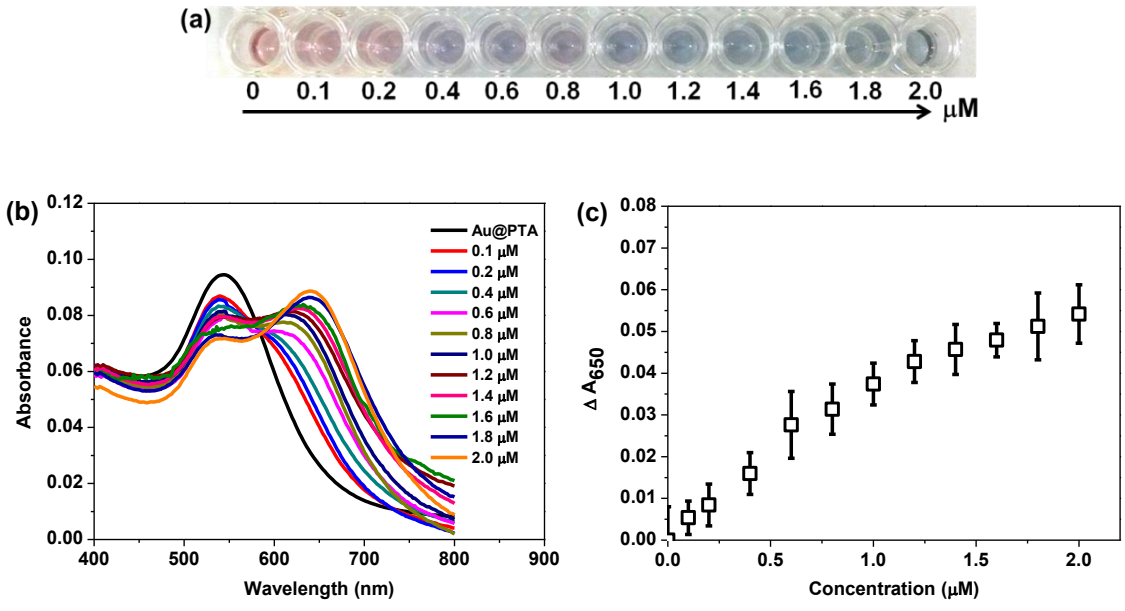

Figure 7. Different concentrations of H_2O_2 were added to a solution containing Au@PTA nanocomposites in DI water. (a) Photograph showing differing colors and intensities of Au@PTA nanocomposites solutions after 5 min of reaction time caused by varying degrees of aggregation. The color of the solution changed from red to blue as the concentration of H_2O_2 increased from 0.1 μM to 2.0 μM. (b) UV–Vis spectra of solution after 5-minute reactions for different H_2O_2 concentrations. The localized surface plasmon resonance peak red shifts when the concentration of H_2O_2 is 0.1 μM or higher. (c) Graph showing absorbance at ~ 650 nm of the various samples reacted with different concentrations of H_2O_2. Values were normalized by subtracting from the A_{650} value at 0 μM H_2O_2 concentration. The error bars represent the standard deviations of three replicates.

Interestingly, while comparing the UV-vis spectrometry of our two assays (Figure 4a and Figure 7a), we realized that as increasing H_2O_2 was added to the H_2O_2 detection assay, a second peak appeared at ~ 650 nm with increasing intensity. This peak was absent in the Fe^{3+} assay regardless of the concentration of Fe^{3+} added. The differing absorbance spectra suggested that different localized surface plasmon resonance (LSPR) coupling events occurred in each of the two assays. For the H_2O_2 detection assay, the second peak at ~ 650 nm was attributed to the formation of aggregates with “wire-like” oligomer structure visible under SEM giving rise to strong interparticle plasmon coupling resulted from the aggregation of adjacent Au@PTA (Figure 8).[36] This contrasted differently to SEM images of the Au@PTA aggregated in the presence of Fe^{3+} (Figure S3). This also explained the high visual detection of sensitivity of H_2O_2 (0.4 μM) as compared to Fe^{3+} (20 μM) in their respective Au@PTA based sensor assays.

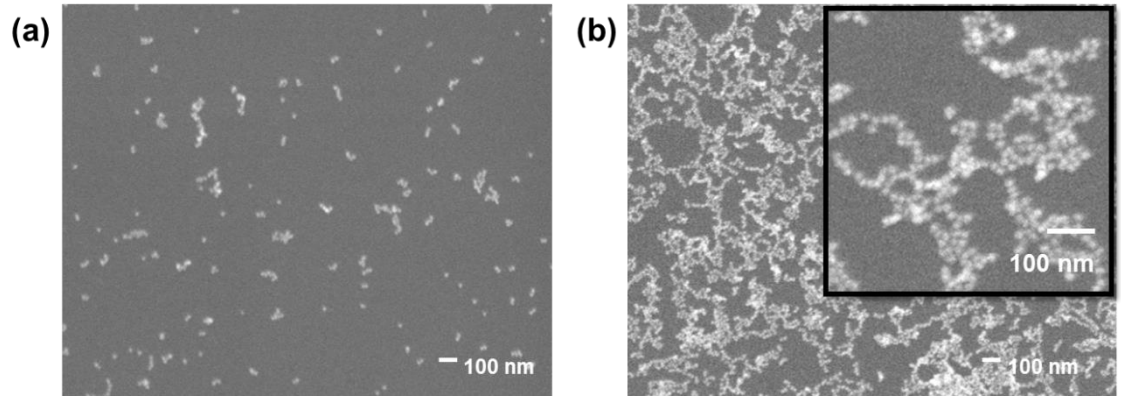

Figure 8. (a) SEM images of Au@PTA nanocomposites + Fe^{2+}. (b) SEM image of the Au@PTA nanocomposites + Fe^{2+} + H_2O_2 with lower and higher magnification (inset).

To account for the "wire-like" oligomer structure present in the H_2O_2 detection assay but absent in the Fe^{3+} detection assay, we examine the chemistry taking place for each assay. In the Fe^{3+} detection assay, the addition of Fe^{3+} Au@PTA resulted in an aggregation induced by the coordination between Fe^{3+} and the galloyl groups of PTA. However, when H_2O_2 was added to the mixture of Au@PTA and Fe^{2+} ions, a multi-step reaction took place. When added, H_2O_2 induced oxidation of Fe^{2+} to Fe^{3+} which was accompanied by the generation of ·OH free radicals (Equation (1)). The ·OH free radicals then reacted with the galloyl groups of PTA by capturing proton from them (Equation (2-3)) converting the polyphenol into phenoxyl radicals. Unlike galloyl groups which coordinated efficiently with Fe^{3+}, no coordination takes place between phenoxyl radicals and Fe^{3+} ions. The absence of galloyl groups which had been replaced with phenoxyl radicals resulted in the slowing down of Au@PTAs aggregation. Thus, the formation and aggregation of oligomers was more favorable than the aggregation of Au@PTAs.

$$Fe^{2+} + H_2O_2 \longrightarrow Fe^{3+} + {}^{\cdot}OH + HO^- \qquad (1)$$

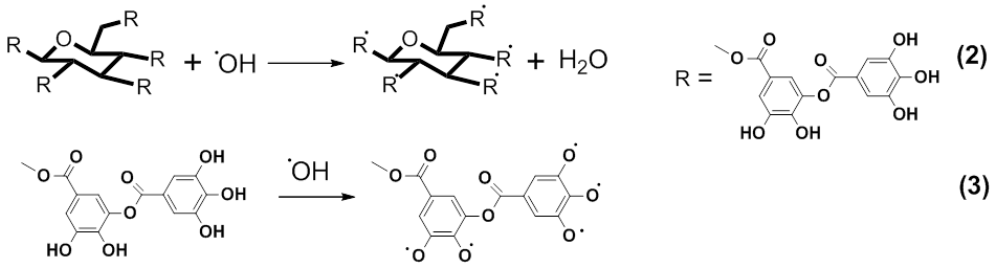

Conclusion

In conclusion, we have developed a highly sensitive Fe^{3+} and H_2O_2 sensor based on Au@PTA core@shell nanocomposites. The one-pot synthesis of Au@PTA was prepared by mixing TA and gold salt together in mildly alkaline pH condition under constant vortex for 20 min at room temperature. TA reduced the gold salt to form AuNP and itself oxidized into PTA. The PTA then assembled onto the AuNP to form Au@PTA nanocomposites.

Relying on Fe^{3+} coordination to galloyl groups on TA, we developed a highly selective and sensitive sensor for detecting Fe^{3+}. The minimum detection limit for naked eye color change from red to blue in the presence of Fe^{3+} only is a hitherto unreported low of 20 μM. Leveraging on the oxidation of Fe^{2+} to Fe^{3+} by H_2O_2, we were able to develop our sensor further to detect H_2O_2 when Au@PTA was mixed together with Fe^{2+}. The naked eye detectable color change for this assay was 0.4 μM of H_2O_2. The high sensitivity of the H_2O_2 assay maybe explained by the formation of "wire-like" oligomer formed due to the presence of phenoxyl groups and the absence of galloyl groups.

As iron and its ions are important biological minerals while H_2O_2 is an important chemical intermediary in various industries, it is imperative that a highly sensitive, selective and easily visible read-out is available to detect the presence of Fe^{3+} and H_2O_2. Herein, we have developed a PTA coated Au core@shell nanocomposite that fulfills these criteria. Coupled with its green, one-pot and one-step synthesis method, our assay is highly advantageous.

Experimental

Materials. Hydrogen Tetrachloroaurate Hydrate ($HAuCl_4 \cdot 3H_2O$), Hydrogen Peroxide (H_2O_2), Trisodium Citrate, Tannic Acid (TA), Sodium Borohydride ($NaBH_4$), Silver Nitrate ($AgNO_3$), Rubidium Chloride (RbCl), Calcium Chloride ($CaCl_2$), Manganese Chloride Tetrahydrate ($MnCl_2 \cdot 4H_2O$), Colbalt(II) Nitrate Hexhydrate ($Co(NO_3)_2 \cdot 4H_2O$), Nickel Sulfate Hexahydrate ($Ni_2SO_4 \cdot 6H_2O$), Copper(II) Sulfate Pentahydrate ($CuSO_4 \cdot 5H_2O$), Zinc Sulfate Heptahydrate ($Zn_2SO_4 \cdot 6H_2O$), Cadmium Chloride ($CdCl_2$), Mercury(II) Chloride ($HgCl_2$), Aluminium Postassium Sulfate Dodecahydrate ($AlKO_8S_2 12H_2O$), Potassium Chromium(III) Sulfate Dodecahydrate ($CrKO_8S_2 \cdot 12H_2O$), Neodymium(III) Chloride Hexahydrate ($NdCl_3 \cdot 6H_2O$), Gadolinium(III) Chloride Hexahydrate ($Cl_3Gd \cdot 6H_2O$), Dysprosium(III) Chloride Hexahydrate ($Cl_3Dy \cdot 6H_2O$), Iron(III) Chloride Hexahydrate ($FeCl_3 \cdot 6H_2O$), and Iron(II) Chloride ($FeCl_2$), were purchased from Sigma-Aldrich, Sodium Chloride (NaCl), Potassium Chloride (KCl) were purchased from Merck. Magnesium Sulfate Anhydrous ($MgSO_4$) was purchased from MP Biomedicals. All chemicals were used as received. Phosphate buffer (PB), sodium salt (pH = 7.8, 10 mM) was used for synthesizing PTA-based core@shell nanocomposites. Water used in all experiments was deionized and ultrafiltered to 18 MΩ·cm using a Milipore Milli-Q gradient system.

Synthesis of core-shell metal@PTA nanocomposites. Au@PTA nanocomposites were prepared by pipetting 50 μL of TA (40 mg mL^{-1}) into 10 mL $HAuCl_4 \cdot 3H_2O$ (1 mM) in 10 mM PB (pH = 7.8) at room temperature in Corning conical tube. It is to be noted that synthesis in other tubes (e.g. BD Falcon) did not yield any nanoparticle. The suspension

was then vigorously mixed with a vortex mixer for 20 min. The color of the solution turned red and gradually deepened until no further color change was observed. The obtained Au@PTA were collected by centrifugation (9000 x g for 15 min) and rinsed with water twice. Bare AuNPs were synthesized with the same method, except that PB solution (pH = 7.8, 10 mM) was replaced with DI water. When conducting pH-dependent experiments, various buffer systems were used to adjust the pH value: pH = 3.3, glycine - HCl (10 mM); pH = 6.0, 7.0, 7.8, PB (10 mM); pH = 8.5, Tris-HCl (10 mM).

Characterization. The size and morphology of the synthesized materials were characterized using field-emission scanning electron microscopy (FE-SEM, JEOL JSM-6700F) at an acceleration voltage of 5 kV, transmission electron microscope (TEM, Hitachi H-7500), and HRTEM with an energy dispersive X-ray spectrometry (HRTEM-EDX, FEI, Tecnai G2 F20). Zeta-potential measurements were conducted in water by a potential analyzer (Zetasizer Nano ZS, Malvern Instruments). UV-Vis absorption tests were carried out on Shimadzu UV-2450 spectrophotometer in transmission mode.

Highly selective visual detection of iron(Ⅲ) cations. The standard procedure is as follows. Briefly, aliquots of 1 mM Fe^{3+} were added to the aqueous Au@PTA solutions (1 mL) to yield the final concentration series (1.0 μM - 400μM). We also investigated the selectivity of our new approach for Fe^{3+} over other metal ions (Na^{+}, K^{+}, Rb^{+}, Ag^{+}, Mg^{2+}, Ca^{2+}, Mn^{2+}, Fe^{2+}, Co^{2+}, Ni^{2+}, Cu^{2+}, Zn^{2+}, Cd^{2+}, Hg^{2+}, Al^{3+}, Cr^{3+}, Dy^{3+}, Gd^{3+}, Nd^{3+}) under the same conditions. The color change from red to blue indicates successful detection of specific ions. It is to be noted that aggregates may form after a few days. UV-Vis spectra were acquired to investigate the interaction between the ions and Au@PTA.

Visual detection of H_2O_2. Au@PTA solution was added to a 96-well plate to a volume of 100 μL. Subsequently, Fe^{2+} was added to final concentration of 20 μM. The reaction was started by adding various volume of 100 μM H_2O_2.

Acknowledgment

This paper was supported by Samsung Research Fund, Sungkyunkwan University, 2015.

Reference

[1] F. Faupel, V. Zaporojtchenko, T. Strunskus, M. Elbahri, Metal-Polymer Nanocomposites for Functional Applications, Adv. Eng. Mater. 12 (2010) 1177-1190.

[2] D. Li, Q. He, J. Li, Smart core/shell nanocomposites: intelligent polymers modified gold nanoparticles, Adv. Colloid Interface Sci. 149 (2009) 28-38.

[3] R. Ghosh Chaudhuri, S. Paria, Core/Shell nanoparticles: classes, properties, synthesis mechanisms, characterization, and applications, Chem. Rev. 112 (2012) 2373-2433.

[4] H. Roghani-Mamaqani, V. Haddadi-Asl, M. Salami-Kalajahi, In situ controlled radical polymerization: a review on synthesis of well-defined nanocomposites, Polym. Rev. 52 (2012) 142-188.

[5] H.J. Kim, Y.S. Choi, M.Y. Lim, K.H. Jung, D.G. Kim, J.J. Kim, et al., Reverse osmosis nanocomposite membranes containing graphene oxides coated by tannic acid with chlorine-tolerant and antimicrobial properties, J. Membrane Sci. 514 (2016) 25-34.

[6] Y.Z. Cao, R.F. Zheng, X.H. Ji, H. Liu, R.G. Xie, W.S. Yang, Syntheses and characterization of nearly monodispersed, size-tunable silver nanoparticles over a wide size range of 7-200 nm by tannic acid reduction, Langmuir, 30 (2014) 3876-3882.

[7] T.Y. Kim, S.H. Cha, S. Cho, Y. Park, Tannic acid-mediated green synthesis of antibacterial silver nanoparticles, Arch. Pharm. Res. 39 (2016) 465-473.

[8] Y. Fang, J. Tan, T. Lan , S.G. F. Foo , D. G. Pyun, S. Lim, D.H. Kim, Universal one-pot, one-step synthesis of core–shell nanocomposites with self-assembled tannic acid shell and their antibacterial and catalytic activities, J. Appl. Polym. Sci. 135 (2018) 45829.

[9] T. Zeng, X.L. Zhang, Y.Y. Guo, H.Y. Niu, Y.Q. Cai, Enhanced catalytic application of Au@polyphenol-metal nanocomposites synthesized by a facile and green method, J. Mater. Chem. A 2 (2014) 14807-14811.

[10] M.J. Behrenfeld, A.J. Bale, Z.S. Kolber, J. Aiken, P.G. Falkowski, Confirmation of iron limitation of phytoplankton photosynthesis in the equatorial pacific ocean, Nature 383 (1996) 508-511.

[11] P.G. Falkowski, R.T. Barber, V.V. Smetacek, Biogeochemical Controls and Feedbacks on Ocean Primary Production, Science 281 (1998) 200-207.

[12] M.A. Smith, P.L. Harris, L.M. Sayre, G. Perry, Iron accumulation in Alzheimer disease is a source of redox-generated free radicals, Proc. Natl. Acad. Sci. U. S. A. 94 (1997) 9866-9868.

[13] O. Blokhina, E. Virolainen, K.V. Fagerstedt, Antioxidants, oxidative damage and oxygen deprivation stress: a review, Ann. Bot. 91 (2003) 179-194.

[14] M.P. Mattson, Pathways towards and away from Alzheimer's disease, Nature 430 (2004) 631-639.

[15] X. Liu, E.C. Theil, Ferritins: dynamic management of biological iron and oxygen chemistry, Acc. Chem. Res. 38 (2005) 167-175.

[16] X.J. Zhao, R.X. He, M. Li, N.W. Zhao, Y.F. Li, C.Z. Huang, Formation of blue fluorescent ribbons of 4', 4""-(1, 4-phenylene) bis (2, 2': 6', 2"-terpyridine) and highly selective visual detection of iron (ii) cations, RSC Adv. 3 (2013) 111-116.

[17] R.L. Liu, H.Y. Lu, M. Li, S.Z. Hu, C.F. Chen, Simple, efficient and selective colorimetric sensors for naked eye detection of Hg^{2+}, Cu^{2+} and Fe^{3+}, RSC Adv. 2 (2012) 4415-4420.

[18] A. Mitra, B. Ramanujam, C.P. Rao, 1-(d-Glucopyranosyl-2′-deoxy-2′-iminomethyl)-2-hydroxynaphthalene as chemo-sensor for Fe^{3+} in aqueous HEPES buffer based on colour changes observable with the naked eye, Tetrahedron Lett. 50 (2009) 776-780.

[19] S.P. Wu, Y.P. Chen, Y.M. Sung, Colorimetric detection of Fe^{3+} ions using pyrophosphate functionalized gold nanoparticles, Analyst 136 (2011) 1887-1891.

[20] D. Wei, Y. Sun, J. Yin, G. Wei, Y. Du, Design and application of Fe3+ probe for “naked-eye” colorimetric detection in fully aqueous system, Sens. Actuators, B 160 (2011) 1316-1321.

[21] X. Chen, X. Zhou, J. Hu, Pt-DNA complexes as peroxidase mimetics and their applications in colorimetric detection of H2O2 and glucose, Anal. Methods 4 (2012) 2183-2187.

[22] K. Nitinaivinij, T. Parnklang, C. Thammacharoen, S. Ekgasit, K. Wongravee, Colorimetric determination of hydrogen peroxide by morphological decomposition of silver nanoprisms coupled with chromaticity analysis, Anal. Methods 6 (2014) 9816-9824.

[23] T. Chen, L. Tian, Y. Chen, B. Liu, J. Zhang, A facile one-pot synthesis of Au/Cu_2O

nanocomposites for nonenzymatic detection of hydrogen peroxide, Nanoscale Res. Lett. 10 (2015) 935.

[24] J. Guan, J. Peng, X. Jin, Synthesis of copper sulfide nanorods as peroxidase mimics for the colorimetric detection of hydrogen peroxide, Anal. Methods 7 (2015) 5454-5461.

[25] L. Guo, A.R. Ferhan, H. Chen, C. Li, G. Chen, S. Hong, et al., Distance-mediated plasmonic dimers for reusable colorimetric switches: a measurable peak shift of more than 60 nm, Small 9 (2013) 234-40.

[26] M. Grzelczak, J. Perez-Juste, P. Mulvaney, L.M. Liz-Marzan, Shape control in gold nanoparticle synthesis, Chem. Soc. Rev. 37 (2008) 1783-1791.

[27] Y. Sun, Y. Xia, Shape-controlled synthesis of gold and silver nanoparticles, Science 298 (2002) 2176-2179.

[28] T.S. Sileika, D.G. Barrett, R. Zhang, K.H.A. Lau, P.B. Messersmith, Colorless multifunctional coatings inspired by polyphenols found in tea, chocolate, and wine, Angew. Chem. Int. Edit. 52 (2013) 10766-10770.

[29] J. Fei, J. Zhao, C. Du, A. Wang, H. Zhang, L. Dai, et al., One-pot ultrafast self-assembly of autofluorescent polyphenol-based core@shell nanostructures and their selective antibacterial applications, ACS Nano 8 (2014) 8529-8536.

[30] M. Jastrzebska, J. Zalewska-Rejdak, R. Wrzalik, A. Kocot, I. Mroz, B. Barwinski, et al., Tannic acid-stabilized pericardium tissue: IR spectroscopy, atomic force microscopy, and dielectric spectroscopy investigations, J. Biomed. Mater. Res., Part A 78 (2006) 148-156.

[31] I. Erel-Unal, S.A. Sukhishvili, Hydrogen-bonded multilayers of a neutral polymer

and a polyphenol, Macromolecules 41(2008) 3962-3970.

[32] L. Lybaert, E. De Vlieghere, R. De Rycke, N. Vanparijs, O. De Wever, S. De Koker, et al., Bio-hybrid tumor cell-templated capsules: a generic formulation strategy for tumor associated antigens in view of immune therapy, Adv. Funct. Mater. 24 (2014) 7139-7150.

[33] D. Gursoy, T. Bicer, J.D. Almer, R. Kettimuthu, S.R. Stock, F. De Carlo, Maximum a posteriori estimation of crystallographic phases in X-ray diffraction tomography, Philos. Trans. A. Math. Phys. Eng. Sci. 373 (2015).

[34] K. Liang, R. Ricco, C.M. Doherty, M.J. Styles, S. Bell, N. Kirby, et al., Biomimetic mineralization of metal-organic frameworks as protective coatings for biomacromolecules, Nat. Comm. 6 (2015) 7240.

[35] D.J. Tobler, J.D. Rodriguez-Blanco, K. Dideriksen, N. Bovet, K.K. Sand, S.L.S. Stipp, Citrate effects on amorphous calcium carbonate (ACC) structure, stability, and crystallization, Adv. Funct. Mater. 25 (2015) 3081-3090.

[36] X. Guo, Y. Ying, L. Tong, Photonic nanowires: from subwavelength wave guides to optical sensors, Acc. Chem. Res. 47 (2013) 656-666.